ELSEVIER

Earth and Planetary Science Letters 193 (2001) 381–394

EPSL

www.elsevier.com/locate/epsl

Hot vents in an ice-cold ocean: Indications for phase separation at the southernmost area of hydrothermal activity, Bransfield Strait, Antarctica

A. Dählmann [a,*], K. Wallmann [a], H. Sahling [a], G. Sarthou [a,1], G. Bohrmann [a], S. Petersen [b], C.S. Chin [c], G.P. Klinkhammer [c]

[a] *GEOMAR, Research Center for Marine Geosciences, Wischhofstrasse 1–3, 24148 Kiel, Germany*
[b] *Freiberg University of Mining and Technology, Department of Economic Geology and Leibniz Laboratory for Applied Marine Research, Institute for Mineralogy, Brennhausgasse 14, 09596 Freiberg, Germany*
[c] *Oregon State University, College of Oceanic and Atmospheric Sciences, 104 Ocean. Admin. Building, Corvallis, OR 97331, USA*

Received 31 January 2001; accepted 1 October 2001

Abstract

During the expeditions ANT-XV/2 with R/V *Polarstern* in 1997/98 and NBP 99-04 with R/V IB *N.B. Palmer* in 1999, the first samples of hydrothermally influenced sediments of Bransfield Strait were obtained at Hook Ridge, a volcanic edifice in the Central Basin of the Strait. The vent sites are characterized by white siliceous crusts on top of the sediment layer and temperatures measured immediately on deck are up to 48.5°C. The shallow depth of these vent sites (1050 m) particularly controls the chemistry of the pore fluids that are enriched in silica and sulfide and show low pH values. Chloride is depleted up to 20% and the calculated hydrothermal endmember concentration is in the range of 1–84 mM. Since other mechanisms for Cl depletion can be ruled out clearly, the composition of this fluid is attributed to phase separation. While the Cl-depleted fluid is emanating at Hook Ridge, a Cl-enriched fluid can be identified in the adjacent King George Basin. Using a *p,x* diagram the two corresponding endmember concentrations reveal that the phase separation takes place at subcritical conditions (total depth: ~2500 m), probably along the whole volcanic edifice.

Keywords: liquid phase; separation; hydrothermal vents; Antarctica; Bransfield Strait

1. Introduction

Phase separation is a widely recognized phenomenon at mid-ocean ridges. The chemical composition of the fluids at hydrothermal vent sites critically depends on the depth at which phase separation occurs (e.g. [1–3]) and the timing of volcanic activity with respect to fluid venting (e.g. [4–9]). Vent sites of the East Pacific Rise (EPR) and the Mid-Atlantic Ridge (MAR) are

* Corresponding author. Present address: Utrecht University, Faculty of Earth Sciences, Department of Geochemistry, P.O. Box 80021, 3508 TA Utrecht, The Netherlands. Tel.: +31-30-253-5037; Fax: +31-30-253-5302.
E-mail address: A.Daehlmann@geo.uu.nl (A. Dählmann).

[1] Present address: IUEM-LEMAR-UMR 6539, Technopole Brest Iroise, Place Nicolas Copernic, 29280 Plouzane, France

0012-821X/01/$ – see front matter
PII: S0012-821X(01)00535-0

typically situated in water depths of 2300–3700 m. The shallowest hydrothermal system that has been intensively studied is located at Axial Seamount on the Juan de Fuca Ridge in a water depth of 1540 m. This system is especially known for its extreme fluid compositions that are attributed to phase separation at shallow depth although additional alteration reactions may also play a role [6,10]. Vents at even shallower depths have been explored on the MAR at 37°50′N (Menez Gwen, 840 m) and at 67°N (Kolbeinsey Ridge, 100 m), but only very few data exist on the chemical composition of their fluids so far. However, phase separation is suggested to occur at both sites [11–13].

In this paper we present investigations on a shallow vent site (1050 m) at Hook Ridge, one of the hydrothermally active areas of the Central Bransfield Strait that have been discovered earlier [14,15]. The reported site was first sampled in 1997 [16] and is the southernmost site of hydrothermal activity known to date. Its specific conditions are indeed unique, not only because of its high latitude but also due to its shallow depth and thin sediment cover.

Bransfield Strait is a marginal basin that is only just on the transition from intracontinental rifting to back-arc spreading and represents an early stage of the evolution of a hydrothermal system. Therefore, this area is of a wider interest to studies on the general development of ridge vent systems.

2. Geological and tectonic setting

Bransfield Strait is a marginal basin located between the Antarctic Peninsula and the South Shetland Islands (Fig. 1); it is about 400 km long and has a maximum width of 80 km. The basin is volcanically and tectonically active and several subaerial and submarine volcanic edifices are situated along and parallel to the major rifting axis. Subduction along the South Shetland trench ceased or at least drastically slowed down about 3–4 Ma BP [17,18], followed by the onset of extension in the back-arc region about 1–2 Ma BP [19], whereas the earliest known back-arc volcanism only began about 0.3 Ma BP and is still active [20]. Due to the lack of active arc volcanism and subduction Bransfield Strait is considered an extensional marginal basin with intracontinental rifting occurring along parallel axes rather than a back-arc basin with seafloor spreading on oceanic crust [16,17,19,21]. In contrast to this tectonic particularity, the geochemistry of dredged rocks of basaltic to basaltic–andesitic composition is similar to other back-arc basalts [19,21].

The investigated volcanic edifice, Hook Ridge, is situated on the central rifting axis of the Central Bransfield Basin at 62°12′S/57°17′W. It reaches a water depth of about 1050 m, whereas the adjacent, flat-bottomed King George Basin is approximately 2000 m deep. The hook-shaped structure is covered with a thin layer of soft diatomaceous mud; bare rocks appear only at steeper flanks.

3. Investigations of hydrothermal activity

Hydrothermal activity within the Bransfield Strait was first documented by thermogenic carbohydrates in the sediment [22–25] and ^{3}He plumes in the water column [26]. Heat flow measurements [20] and further investigations of water column anomalies (temperature, Mn, particles) verified the existence of active hydrothermal activity in this area [14,15].

During the expeditions ANT-XV/2 with R/V *Polarstern* in 1997/98 (ANT) and NBP 99-04 with R/V IB *N.B. Palmer* in 1999 (NBP), we carried out detailed investigations of the seafloor and water column at Hook Ridge using a video-guided camera sled (OFOS), a video-guided grab sampler (TVG), and a towed instrument package (ZAPS). Details of the deployed instruments and water column anomalies (T, CH_4, Mn, turbidity) are reported in [16] and [27].

All vent sites were situated on the ridge crest (Fig. 1, Table 1) and were characterized by white siliceous crusts on top of the sediment layer (see photograph in [16]). The memory CTD mounted on OFOS recorded elevated temperatures in the water column 2–4 m above the white patches. The highest T anomalies coincide with Fe, Mn, and turbidity plumes measured with the ZAPS system

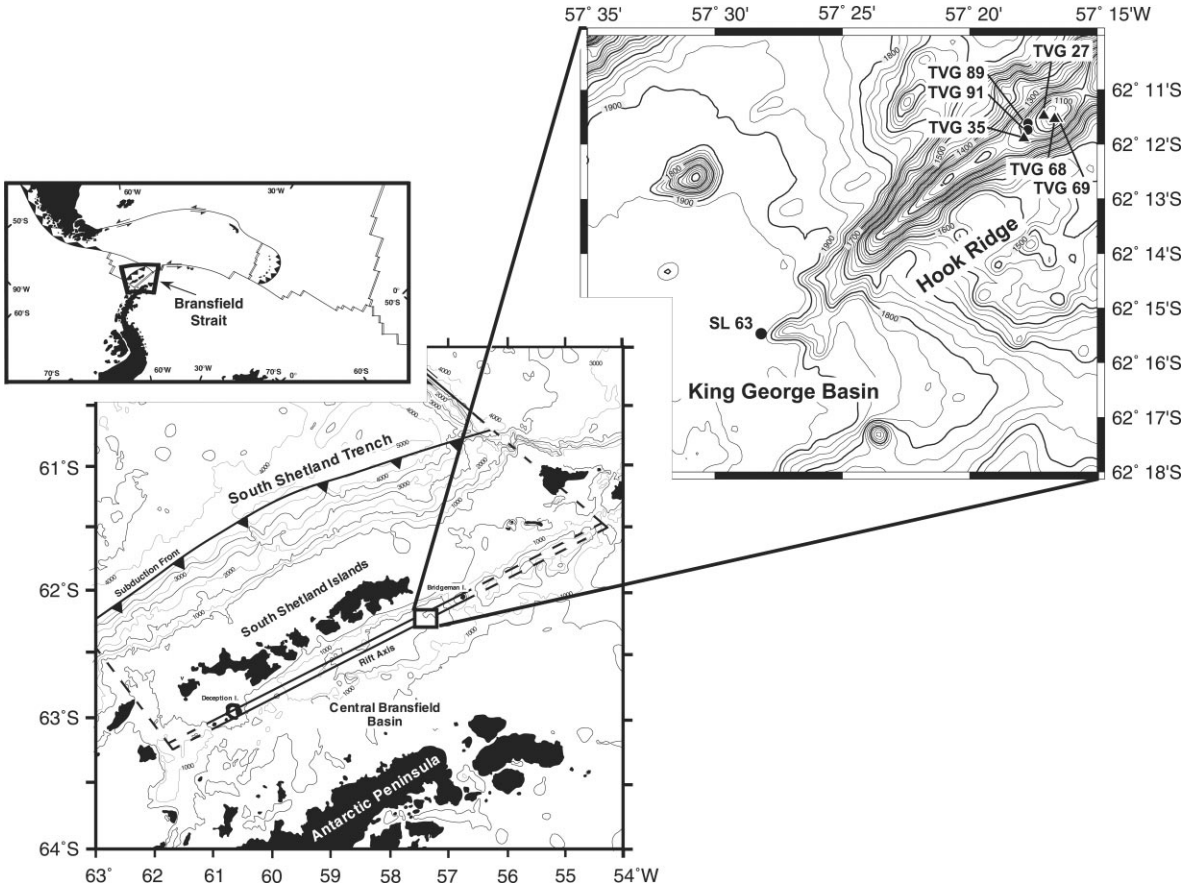

Fig. 1. Bathymetric map of the area of investigation, Hook Ridge, within its tectonic setting of Bransfield Strait.

at the same location [27] and were detected within a crater-like structure with fairly steep inner walls. In the SW corner of this feature, we sampled the warmest sediments with temperatures of 48.5°C (NBP-TVG 68) and 42°C (NBP-TVG 69), respectively. The sediment underneath the silica cover of NBP-TVG 69 had a soupy consistency and also contained a ~25 cm thick ash layer. In contrast to other hydrothermal systems, vent fauna was not observed at this site.

Table 1
Synopsis of reported vent (vent) and reference (ref.) sites sampled by TV-grab at Hook Ridge during cruises ANT-XV/2 with R/V *Polarstern* (ANT) and NBP 99-04 with R/V IB *N.B. Palmer* (NBP) with maximum temperature, core location and water depth

Cruise-station	Max. temperature (°C)	Latitude (°S)	Longitude (°W)	Water depth (m)
ANT-TVG 89 (ref.)	–	62°11.64′	57°17.67′	1134
ANT-TVG 91 (vent)	24	62°11.80′	57°17.67′	1133
NBP-TVG 27 (ref.)	–	62°11.45′	57°17.07′	1058
NBP-TVG 35 (vent)	11	62°11.86′	57°17.87′	1162
NBP-TVG 68 (vent)	48.5	62°11.51′	57°16.62′	1052
NBP-TVG 69 (vent)	42	62°11.53′	57°16.68′	1045

4. Sampling and analytical methods

The sediment temperature was measured with a conventional thermometer directly within the sediment immediately upon recovery of the TV-grab sampler. Subsamples were taken with plastic tubes and the pore water was separated from the sediment using a Teflon squeezer under inert gas atmosphere. The pH of bulk sediment was measured with a glass electrode prior to squeezing, with buffers prepared in artificial seawater [28]. Analyses of dissolved silica and sulfide were carried out directly after pore water extraction by standard photometric methods [29], with some modifications for samples with high sulfide content. Mg and Ti were analyzed by inductively coupled plasma-atomic emission spectrometry (ICP-AES); Cl^-, Br^-, and SO_4^{2-} by ion chromatography, both in the laboratories of GEOMAR. Selected solid phase samples of the ANT cruise were also analyzed for their Mg concentration using X-ray fluorescence analysis (XRF) at TU Freiberg. Isotopic analyses of pore waters ($\delta^{18}O$, δD) were carried out by mass spectrometry at an external laboratory (Geochemische Analysen, Sehnde).

5. Results and discussion

5.1. Pore water characteristics and calculation of the Cl endmember concentration

The substantial characteristics of hydrothermal influence are high silica concentrations (up to $\sim$2.4 mM), sulfide enrichments (up to $\sim$1 mM), Br^- and Cl^- depletions (Cl^- down to 442 mM), and low pH values ($\sim$5) (Table 2, see also [27]). Both Mg and sulfate are depleted significantly in NBP-TVG 68 and 69 compared to the reference site.

In analogy to hydrothermal fluids, pore waters at sedimented hydrothermal sites are generally assumed to be a mixture of hydrothermal fluid and diagenetically altered pore water. As Mg has been shown to be totally removed from solution during basalt–seawater interaction [30,31], calculations of endmember concentrations are commonly done by extrapolation to zero Mg. However, these calculations can also be made assuming an endmember fluid of zero sulfate concentration, since sulfate is likewise quantitatively removed within the recharge zone of a hydrothermal circulation cell as has been shown for many sites [32]. In contrast to sediment-starved systems, both Mg^{2+} and SO_4^{2-} are subject to diagenetic reactions at sedimented sites, which requires particular consideration. During the degradation of organic matter sulfate is reduced to sulfide and Mg^{2+} may be desorbed from the sediment by cation exchange [33] or leached from the matrix by the hot and acid fluids. XRF measurements of Hook Ridge sediments reveal that almost half of the Mg content has been leached by hydrothermal alteration; e.g. at vent site ANT-TVG 91 the Ti-normalized Mg content is 3.5 ± 0.2 (on a molar basis), compared to 6.5 ± 0.4 at reference site ANT-TVG 89. Under these circumstances, the working assumption of zero Mg in the endmember fluid is not applicable. We therefore assume an endmember fluid with zero sulfate. If sulfate reduction is a relevant process within the sediment column under consideration (50 cm), this procedure would result in an overestimation of the hydrothermal fluid component.

We apply two different approaches for calculation of the hydrothermal endmember concentration: simple two-component mixing and linear extrapolation. For mixing we chose the deepest pore water sample from NBP-TVG 68, which has the lowest concentrations of Mg (43.7 mM), SO_4^{2-} (21.9 mM), and Cl^- (442 mM) and, hence, is the sample with the highest content of hydrothermal component. The sulfate concentration of this pore water sample can be obtained by mixing seawater (28.9 mM SO_4^{2-}) with 24% of a hydrothermal endmember with zero SO_4^{2-} concentration. From this mixture and a bottom water Cl^- concentration of 555 mM, the calculated endmember concentration for Cl^- is 84 mM. The second approach is illustrated in Fig. 2 and includes pore water samples from all NBP-TVG stations. Linear regression of Cl^- versus SO_4^{2-} of all stations but TVG 69 yields a Cl^- endmember concentration of 1 ± 10 mM. With respect to the TVG 68 sample taken for the mixing approach, this result is

Table 2
Compilation of concentrations of pore water constituents and pH of the sediments

Depth (cmbsf)	$Si(OH)_4$ (μM)	ΣH_2S (μM)	Cl (mM)	Br (μM)	SO_4 (mM)	Mg (mM)	pH
ANT-TVG 89 (reference)							
1.0	579	bdl	556	857	27.7	53.1	7.52
3.0	591	bdl	554	841	27.8	na	7.50
5.0	579	bdl	556	840	27.1	53.1	7.53
7.0	601	bdl	554	844	27.7	52.7	7.59
9.0	631	bdl	556	840	27.7	53.6	7.59
11.0	639	bdl	556	845	27.4	52.2	7.61
13.0	619	bdl	552	756	27.1	52.9	7.61
15.0	638	bdl	554	843	27.2	52.3	7.59
17.0	644	bdl	554	842	27.4	53.4	7.61
19.0	644	bdl	552	838	26.9	52.3	7.59
21.0	654	bdl	553	839	26.6	52.4	7.61
23.0	644	bdl	555	839	27.5	na	7.59
25.0	631	bdl	553	836	26.7	52.6	7.61
27.0	645	bdl	552	845	27.8	52.8	7.59
29.0	658	bdl	553	785	25.8	52.7	7.57
31.0	671	bdl	554	905	27.0	52.6	7.57
33.0	692	bdl	552	905	27.0	52.7	7.59
35.0	664	bdl	551	915	27.6	53.0	7.57
37.0	672	bdl	549	540	25.1	na	7.57
39.0	699	bdl	551	909	26.9	52.9	7.59
41.0	677	bdl	552	913	27.6	52.2	7.57
43.0	675	bdl	550	894	26.8	53.0	7.55
45.0	648	bdl	551	780	26.7	na	7.55
47.0	657	bdl	546	846	26.5	52.4	7.63
49.0	657	bdl	548	855	27.2	52.2	7.59
ANT-TVG 91 (vent, 24°C)							
1.0	1364	475	536	827	27.3	51.7	5.57
3.0	1356	538	534	768	26.1	52.3	5.57
5.0	1370	623	535	824	27.4	50.3	5.50
7.0	1370	324	535	823	27.9	51.0	5.49
9.0	1384	509	535	801	27.4	51.4	5.50
11.0	1384	520	535	829	28.0	52.1	5.52
13.0	1392	604	535	817	27.1	51.9	5.46
15.0	1395	579	533	829	27.8	52.3	5.55
17.0	1395	635	532	829	28.0	51.2	5.46
19.0	1420	589	535	827	27.6	52.1	5.50
21.0	1418	601	535	807	27.9	51.4	5.50
23.0	1392	514	534	812	27.1	52.5	5.53
25.0	1387	409	533	850	28.1	50.9	5.47
27.0	1398	377	533	855	27.5	52.3	5.53
29.0	1378	415	532	866	28.1	52.4	5.77
31.0	1412	536	536	870	27.6	52.7	5.70
33.0	1426	566	533	na	na	50.7	5.60
35.0	1429	475	533	819	26.9	51.4	5.46
37.0	1437	541	532	809	27.2	52.0	5.46
39.0	1465	548	535	814	27.3	52.3	5.47
41.0	1448	476	534	814	27.7	52.6	5.49
43.0	1434	423	533	813	27.1	50.6	5.50
45.0	1429	565	532	815	27.7	51.3	5.77
47.0	1415	500	532	821	27.3	51.8	5.75
49.0	1297	403	na	817	28.1	50.6	6.15

Table 2 (*continued*)

Depth (cmbsf)	$Si(OH)_4$ (μM)	ΣH_2S (μM)	Cl (mM)	Br (μM)	SO_4 (mM)	Mg (mM)	pH
NBP-TVG 27 (reference)							
0.5	682	bdl	538	810	26.5	55.2	8.23
1.5	481	bdl	543	820	27.0	54.6	7.79
2.5	895	bdl	532	819	26.6	53.6	7.71
3.5	542	bdl	532	808	26.7	55.0	7.71
4.5	646	bdl	524	796	25.8	54.7	7.68
5.5	672	bdl	536	815	26.6	55.2	7.71
6.5	559	bdl	529	815	26.3	na	7.81
7.5	708	bdl	531	805	26.4	53.9	7.75
8.5	656	bdl	520	796	25.8	54.1	7.71
9.5	704	bdl	524	797	26.0	54.8	7.71
11.5	572	bdl	543	831	27.0	53.8	7.68
14.5	776	bdl	520	783	25.6	55.4	7.97
17.5	636	bdl	532	797	26.2	54.8	7.75
20.5	928	bdl	529	811	26.2	53.0	7.68
23.5	892	bdl	531	811	26.3	54.6	7.68
26.5	925	bdl	523	793	25.7	54.1	7.68
29.5	688	bdl	537	806	26.4	54.7	7.66
32.5	740	bdl	531	812	26.2	54.8	7.68
35.5	711	bdl	524	804	25.9	53.9	7.73
38.5	763	bdl	526	803	25.9	54.1	7.71
41.5	646	bdl	511	761	25.1	54.3	7.71
NBP-TVG 35 (vent, 11°C)							
1.5	1244	482	502	760	25.0	53.2	5.25
4.5	1407	698	505	762	24.8	50.7	4.93
7.5	1603	723	502	772	25.1	49.9	4.88
10.5	1468	628	508	766	24.8	50.9	4.88
13.5	1373	276	498	752	25.0	50.2	4.91
16.5	1231	383	495	742	24.1	50.7	4.93
19.5	1346	436	499	741	24.5	50.8	4.93
22.5	1234	433	492	739	24.1	50.9	4.91
25.5	1285	449	495	722	24.5	47.8	4.91
28.5	1444	385	486	729	23.8	51.6	4.82
31.5	1140	143	471	695	22.9	51.1	4.88
NBP-TVG 68 (vent, 48.5°C)							
1.5	1575	119	483	740	23.8	44.3	5.31
5.0	1987	142	472	717	23.4	na	5.21
8.5	na	na	474	719	23.5	na	5.11
12.0	2151	249	464	695	23.2	43.3	5.05
16.0	2439	320	448	679	22.4	42.9	5.01
19.5	2020	319	454	684	23.1	43.4	5.01
23.0	1987	288	454	684	22.5	43.8	5.03
26.5	2003	327	455	675	22.6	44.1	5.03
30.0	1485	384	450	687	22.3	43.7	5.01
35.0	1707	358	447	669	22.1	43.6	4.98
41.0	1641	355	444	657	22.1	43.8	4.96
46.0	2127	339	442	669	21.9	43.7	4.94
NBP-TVG 69 (vent, 42°C)							
3.0	1936	791	460	673	23.1	45.2	na
12.0	2412	1076	455	675	22.9	45.2	na
19.0	2317	1115	449	626	22.9	42.4	na
26.0	2051	1147	455	686	22.9	45.8	na
30.0	2161	1086	452	661	23.2	44.5	na
37.0	2204	674	454	674	23.0	44.8	na

cmbsf: cm below seafloor; na: not analyzed; bdl: below detection limit.

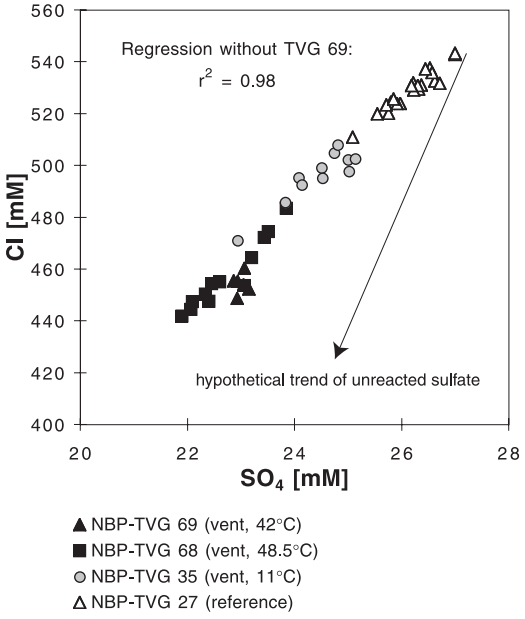

Fig. 2. Correlation of Cl^- with sulfate for calculation of Hook Ridge hydrothermal fluid endmember concentration of Cl^-. Data for all NBP-TVG stations are shown, but data for NBP-TVG 69 are not included in the regression (see text for explanation). The extrapolated Cl^- endmember concentration (zero sulfate) is 1 ± 10 mM. The arrow indicates a hypothetical trend if the measured sulfate concentration was the result of sulfate reduction. If so, the concentration of the unreacted sulfate would be higher, resulting in a steeper Cl^-/SO_4^{2-} gradient and, consequently, an even smaller (i.e. negative) Cl^- endmember concentration.

equivalent to a mixture of 20% hydrothermal component (1 mM) with 80% bottom water (555 mM). The extremely low Cl^- endmember concentration clearly rules out a contribution of diagenetic sulfate reduction. If the measured sulfate concentration was the result of a sulfate reduction, the original SO_4^{2-} concentration would be higher. Hence, with the chlorinities of the pore waters remaining unchanged the Cl^- endmember concentration inferred from the Cl^-/SO_4^{2-} correlation would be even more depleted (indicated schematically by the arrow in Fig. 2). Ex situ oxidation of sulfide can alter the sulfate concentration as an artefact of pore water sampling. This is assumed to be the case for TVG 69, which is therefore excluded from the regression.

To summarize, the endmember calculation results in a percentage of 20–24% for the hydrothermal component and, accordingly, a Cl^- concentration of 1–84 mM. The range in endmember concentrations for Cl^- is due to the fact that these calculations are very sensitive to small changes in the endmember composition.

5.2. Phase separation

Phase separation takes place in the oceanic crust if a hydrothermal fluid (evolved seawater) encounters the two-phase boundary as illustrated in the phase diagram (Fig. 3). The common preceding process is entrainment of seawater into the crust where it is heated, eventually expands, and ascends to the seafloor due to buoyancy forces becoming predominant (adiabatic decompression). This process establishes a hydrothermal convection cell.

The two phases separated along the two-phase curve are often referred to as vapor and brine,

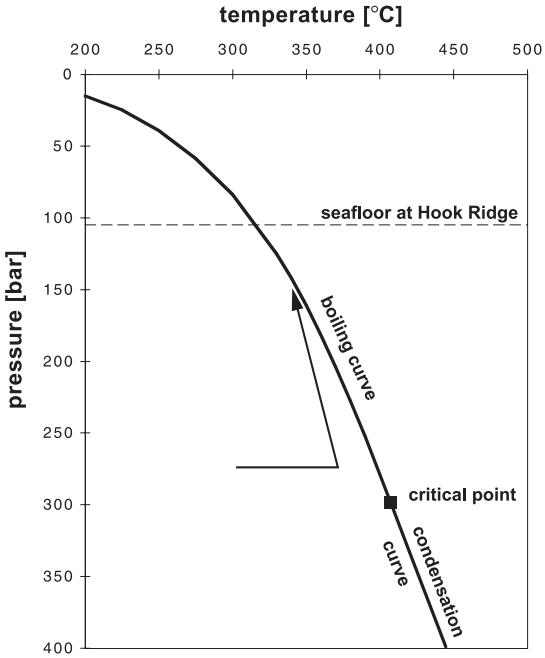

Fig. 3. p,T Diagram for seawater (3.2 wt% NaCl). Data for two-phase boundary curve and critical point (407°C/298.5 bar) from [35]. Dashed line indicates pressure at seafloor depth at Hook Ridge (1050 m). The arrow signifies the p,T changes of circulating seawater, its relative position to the critical point is arbitrary. Phase separation takes place where it encounters the two-phase curve (see text for explanation).

although their chemical composition and salt content vary greatly according to the *p,T* conditions at which the phase boundary is encountered. While both phases have the same salinity at the critical point, the salinities of the separated phases vary significantly at higher and lower *p,T* conditions [34,35]. At higher *p,T* (supercritical conditions) small amounts of a very dense brine will condensate leaving the remaining vapor with a considerable salinity. With increasing depth/pressure of phase separation the segregated vapor phase reaches almost seawater salinity. On the other hand, at lower *p,T* (subcritical conditions) the vapor generated due to boiling has very low salinity. The lower the depth/pressure of phase separation, the more depleted is the vapor in salt content. The resulting liquid phase ('brine') increases in salinity in proportion to the amount of vapor generated and removed. The *p,T*–salinity relationship is treated further below to estimate the depth of phase separation.

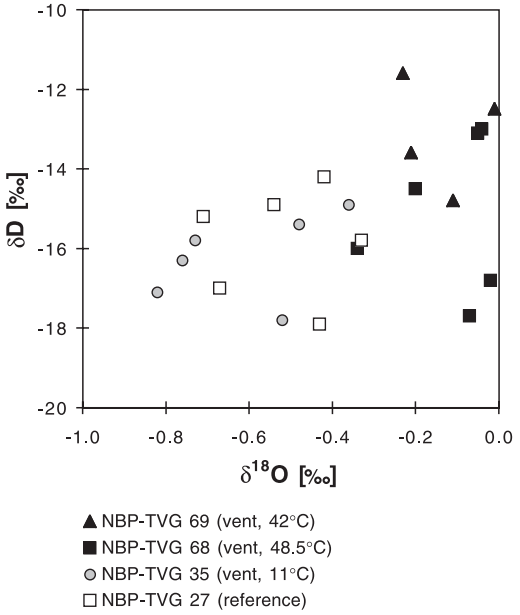

Fig. 4. Isotopic ratios of oxygen and deuterium of pore water samples from all NBP stations; values in ‰ deviation from SMOW. No difference in δD and just a slight difference in $\delta^{18}O$ between vent site and reference site samples clearly show that there is no relevant input of magmatic or meteoric waters.

5.3. Evidence for phase separation

5.3.1. Cl depletion

The striking evidence for phase separation at Hook Ridge is the Cl-depleted pore waters with a deviation from seawater of up to 20% (NBP-TVG 68). Because laboratory experiments on basalt alteration have shown a maximum depletion of Cl in the fluid of 7% [36], Cl depletions greater than 10% are assumed to be due to phase separation (e.g. [2,7]). To fully ascribe the observed Cl depletion to phase separation, other mechanisms also causing decreases in Cl concentration have to be considered and eventually regarded as negligible.

Influence of meteoric or magmatic waters: As meteoric and magmatic waters have different deuterium and oxygen isotopic ratios compared to seawater, an input of one of these waters should result in a shift of the $\delta^{18}O$ and δD values [37,38]. Isotopic analyses, however, reveal essentially equal signatures for δD and only slightly elevated $\delta^{18}O$ for the vent compared to the reference site (Fig. 4). Due to the very low water content of basaltic rocks ($\sim$0.2% to $>$1% at subduction-related settings [39]), dehydration is not likely to release a sufficient amount of water. Additionally, magmatic waters have low Br/Cl ratios, which would decrease the ratio of the fluid [9,40,41] which is also not observed (Fig. 5). These findings clearly rule out the influence of magmatic or meteoric waters on Cl depletion.

Precipitation of Cl-bearing minerals: When Cl is taken up into secondary mineral phases, the Br/Cl ratio of the fluid is altered significantly (e.g. [9,42]). In most of the cases, Cl is preferentially partitioned into the mineral resulting in an increase of Br/Cl with decreasing Cl concentration. The average of Br/Cl data of both pore waters and local bottom water (Fig. 5), however, shows only a slight deviation from the global mean of seawater ($1.51 \pm 0.03 \times 10^{-3}$ compared to $1.55 \pm 0.04 \times 10^{-3}$ for the global mean [40]), considering the errors given. All samples scatter within a $\pm$3% divergence around their mean (dashed lines). The measured values are in very good agreement with high temperature fluids from Axial Seamount ($1.50 \pm 0.05 \times 10^{-3}$ [10]) and North

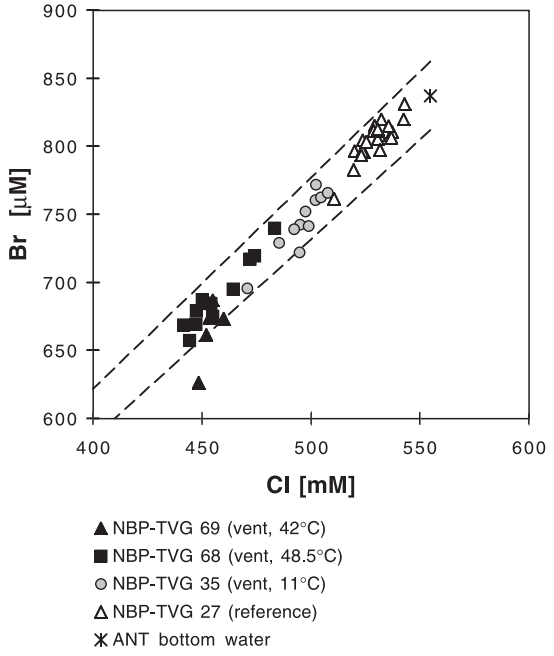

Fig. 5. Correlation of bromide and chloride of pore water samples from all NBP-TVG stations and local bottom water in King George Basin (cruise ANT-XV/2). Dashed lines are divergence of 3% from the average ratio of $1.51 \pm 0.03 \times 10^{-3}$. This constant Br/Cl ratio for both vent and reference site samples precludes a significant uptake of Cl by minerals at the vent site.

Cleft segment ($1.48–1.51 \times 10^{-3}$ [8]), both at Juan de Fuca Ridge. The narrow range of measured values and the small deviation from seawater preclude a significant Cl uptake by minerals and is consistent with Cl depletion caused by phase separation.

5.3.2. Content of dissolved gases

If the emanating fluids are considered to be the vapor phase of a hydrothermal fluid separated at low pressures, they should contain significant amounts of dissolved gases (e.g. [6,7]). The measured concentrations of dissolved sulfide (at low pH mostly as H_2S) show large enrichments at the vent sites (Table 2). Taking the maximum value of $\sim$1 mM and assuming the percentage of endmember fluid is 22%, the endmember concentration of H_2S is calculated to be $\sim$4.5 mM. This is at the lower limit of what is usually observed for Cl-depleted endmember fluids [5,7,8], which is remarkable, because we are dealing with pore waters from sediment. During the pore water extraction, especially at low pH values, dissolved gases are partitioned into the gas phase and thus are irreversibly removed. All concentrations of pore water constituents that are in equilibrium with a gaseous species (HS^-/H_2S, HCO_3^-/CO_2) are therefore minimum values. Taking this artefact into account, the concentrations of gases in the pore water are easily imaged to be as high as any vent fluid with Cl depletion previously measured (e.g. up to 12 mM H_2S at EPR, 18 mM H_2S at the ASHES vent field [43]).

5.3.3. Corresponding 'brine' phase

While the low-chlorinity vapor phase ascends immediately, the corresponding liquid phase ('brine') may accumulate within the crust before being expelled [3,44,45]. To investigate Cl concentration at greater depth we deployed a gravity corer adjacent to Hook Ridge in the King George Basin (ANT-SL 63, cf. Fig. 1) where the sediment–basement interface is at about 50 mbsf [22]. This core shows strong hydrothermal influence inferred from petroleum accumulation and decreasing strontium isotopic ratios with depth (A. Dählmann, unpublished data). Cl concentrations of the pore waters increase with depth reaching a maximum of 579 mM at 6 m (Fig. 6). At this site, pore water concentrations of the upper sediment column are strongly influenced by diagenetic sulfate reduction, precluding extrapolation versus SO_4 for Cl endmember calculation, but Mg is not released from the sediment at this environment. Hence, the Cl endmember concentration, determined by extrapolation to zero Mg, is 703 ± 12 mM (Fig. 6).

5.4. Depth and temperature of phase separation

To estimate the depth of phase separation we use a *p,x* diagram (Fig. 7) drawn from the data given in [46]. The pressure–salinity relationship is characterized by a single salinity at the critical pressure (inflection of the curve) and diverging salinities for decreasing depths. Dashed lines indicate the correspondent pressure of the two-phase boundary curve and x values at intersec-

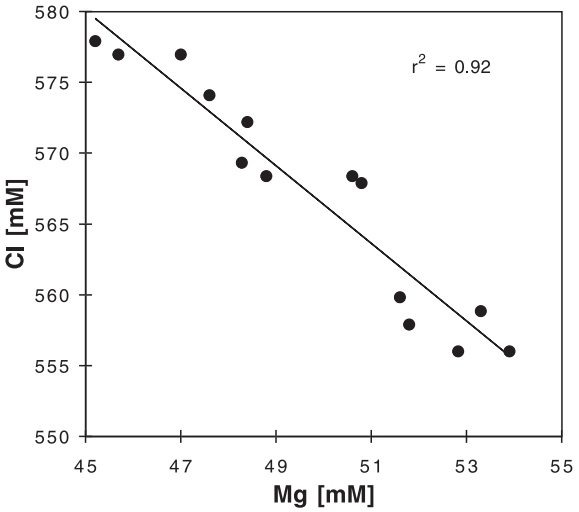

Fig. 6. Correlation of Cl^- with Mg for endmember calculation of a deep-seated brine in King George Basin at the base of the hydrothermally influenced core ANT-SL 63. Calculated Cl^- endmember concentration is 703 ± 12 mM.

tions of the two lines give the salinities of segregated phases.

The calculated endmember of about 1–84 mM for the vapor and 703 mM for the liquid phase fit best with the 390°C isotherm, with a vapor concentration of 65 mM and a liquid concentration of 653 mM at the boiling point. The isotherms for 380°C and 400°C reveal a liquid concentration too low (521 mM) and vapor concentration too high (197 mM), respectively. As the isotherms are only given in 10°C intervals in [46], the conditions at the reaction zone cannot be interpolated more closely and might deviate from the given results by some degrees and bars, because the x values are very sensitive to p,T changes.

The T,x data suggest that the phase separation takes place at subcritical conditions at a total depth of about 2500 m (250 bar), assuming hydrostatic pressure also within the crust [43]. Considering the different water depths (1050 m at Hook Ridge and 2000 m in the King George Basin) and the sediment layer in the basin (50 m), the total depth of 2500 m is achieved about 1450 m within the crust at Hook Ridge and 450 m in the basin. We therefore assume that phase separation occurs underneath Hook Ridge, extending along the strike of the whole volcanic edifice as far as to station SL 63 (Fig. 8). The vapor phase is advecting vertically and expelled at the top of Hook Ridge (TVG stations) whereas the 'brine' phase accumulates in the upper crust and Cl is transported diffusively through the sediment cover of the King George Basin. The very shallow depth of phase separation (500 mbsf in the basin) is a possible scenario because intracrustal diapirism is a typical feature in Bransfield Strait [17] and phase separation at depths as shallow as <200 mbsf has been reported elsewhere [47]. Since the 'brine'-revealing sediment core in the King George Basin is situated in the prolongation of

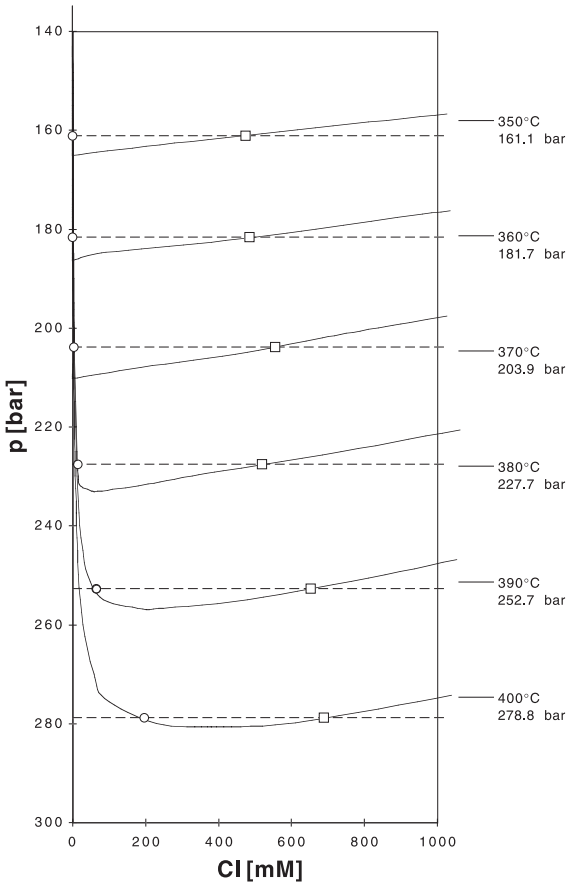

Fig. 7. p,x Diagram for NaCl–H_2O solutions for six isotherms, data for the curves from [46]. Dashed lines indicate corresponding pressures of the two-phase boundary for seawater calculated from the $p(T)$ equation given in [35]. x values at intersections with the isotherms give the salinities of segregated phases at the annotated p,T conditions (circles for vapor and squares for brine phase).

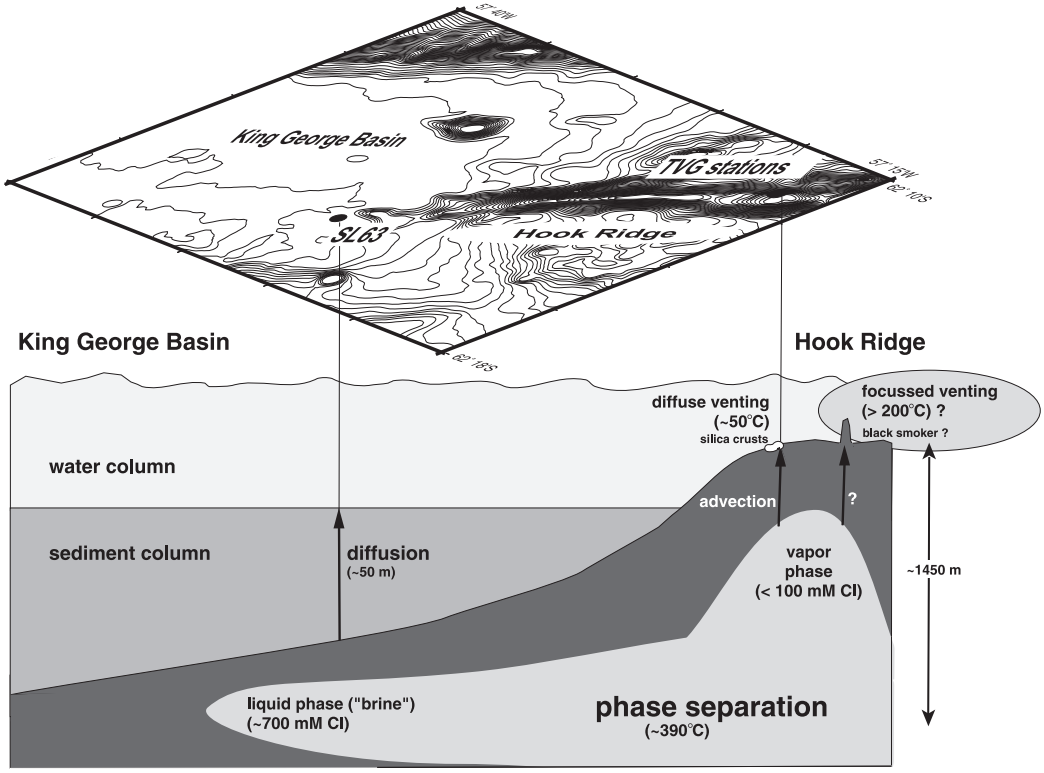

Fig. 8. Schematic section along strike of the rift axis at Hook Ridge and the northern part of the adjacent King George Basin to illustrate phase separation processes. Proportions of the various features are not to scale.

the volcanic structure at the base of Hook Ridge, the two locations are considered as parts of one large volcanic–hydrothermal system, with the vents at the top of Hook Ridge being the sites of active fluid emanation.

5.5. Temperature and manifestation of venting

The visible manifestations of the diffuse fluid venting at Hook Ridge are white silica crusts (opal-A) that precipitated directly above the sediment as well as within the pore space, especially within coarse-grained ash layers through which the fluids probably spread. Calculations on silica solubility (after [48]) reveal that the measured Si concentration in the pore water (NBP-TVG 69) is in approximate equilibrium with amorphous silica at the measured ex situ temperature of 42°C. From the analyses of $\delta^{18}O$ of SiO_2 from this grab an in situ temperature of about 38°C is calculated. Both methods demonstrate that heaving through the cold water column (~ -1.5°C) does not reduce the pore water temperature significantly, owing to the large volume of the retrieved sediment block (~ 1 m^3) and the compact shape of the grab sampler with a small surface/volume ratio. The measured ex situ temperatures are, therefore, likely very close to the in situ temperatures.

Apart from siliceous crusts and small Fe-oxide stubs, no other seafloor manifestations of fluid venting were observed during the video-sled surveys. The lack of further observations can be attributed to several reasons:

1. Subcritical phase separation at shallow depth produces a vapor phase with extremely low concentrations of sulfide-forming metals. This is due either to the high degree of boiling at these con-

ditions or to the low temperature itself. In the first case, the metals are effectively partitioned into the remaining liquid phase while the fluid is boiling. In the second case, they precipitate at greater depth while the fluid is cooled during adiabatic ascent. In either case, the vent fluids do not build visible edifices and diffuse low-temperature emanations dominate the hydrothermal flux even at bare rock sites [8,43,47].

2. At sedimented sites, the sediment layer inhibits a rapid ascent of the fluid and causes a more effective cooling by mixing with the ambient pore water. If the fluid still bears higher amounts of potential chimney-forming minerals when entering the sediment column, they will largely be precipitated within the sediments as has been shown for the Middle Valley site at the Juan de Fuca Ridge [49]. However, at other sedimented ridges such as Guaymas Basin and Escanaba Trough hydrothermal chimneys also occur [50,51]. At Hook Ridge, the only surface expression of hydrothermal activity is concretionary encrustations of metal sulfides (marcasite and pyrite) within the sediment matrix, obviously precipitating along burrow traces that probably served as fluid conduits (ANT-TVG 91 [16]).

3. Talus pieces of former chimney fragments have been found buried within the sediment. Their mineralogy indicates fluid temperatures in excess of 250°C during the formation of the chimney [27]. Additionally, Mn and *T*/*S* water column anomalies detected during cruise NBP 99-04 clearly indicate the presence of high-temperature hydrothermal activity at this site [27]. Thus, besides geological reasons for the absence of active chimneys at Hook Ridge, the lack of finding active vents might simply be due to their scarcity and small spatial scale.

6. Conclusion

With the discovery of thinly sedimented vent sites at Hook Ridge and the investigations of the pore water chemistry we can unequivocally verify the existence of phase separation in Bransfield Strait. The calculated Cl concentrations are among the lowest measured at any MOR site (< 100 mM). To our knowledge there is no other location where phase separation has been invoked from pore water data at a sedimented site although fluid chemistry at Guaymas Basin and Escanaba Trough is consistent with phase separation [52].

Although chimney-like sulfides were found within the sediment column and evidence for active high-temperature venting is given by water column plumes [27], no active hot vent site has yet been directly observed. Cruises ANT-XV/2 and NBP 99-04 reported here are part of the ongoing research in Bransfield Strait and the first with video and camera systems. Our findings suggest that black-smoker-type vents remain to be discovered within Bransfield Strait.

Acknowledgements

We wish to thank E. Suess (GEOMAR) and P. Stoffers (Institute of Geosciences, University of Kiel) for getting funds for the cruise ANT-XV/2. P. Stoffers made the OFOS and TVG systems available for both cruises and D. Garbe-Schönberg (Institute of Geosciences, University of Kiel) assisted in getting funds for the participation of A.D., H.S., and G.S. in cruise NBP 99-04. During cruise ANT-XV/2, many people contributed to finding and sampling the first vent site at Hook Ridge – thanks to them all. We are especially grateful for excellent technical support at sea by B. Domeyer, F. Kulescha, M. Schumann, and the bathymetry group of the Alfred-Wegener-Institute. R. Keller (Oregon State University) and F. Smith (University of Chile) are thanked for their patience and fruitful discussions in front of the OFOS screen during cruise NBP 99-04, as well as C. Wilson and colleagues for their work on water column plumes. Excellent technical support was given by V. Nuppenau and the Antarctic Support Associates. This study was funded by the Federal Ministry of Education and Research (BMBF) Grant 03G0531A/4, German Science Foundation (DFG) Grant WA 1083/1, and National Science Foundation (NSF) Grants OPP 97-31695, OPP-9813450, and OPP-9996238. For analyses at GEOMAR we thank A. Bleyer (IC)

and R. Surberg (ICP-AES). The captains and crew members of the vessels R/V *Polarstern* and R/V IB *N.B. Palmer* are thanked for their support at sea. The manuscript was greatly improved by critical and thoughtful reviews by M. Haeckel, D. Butterfield, J. Bischoff, and an anonymous reviewer. ***[EB]***

References

[1] K.L. Von Damm, J.L. Bischoff, Chemistry of hydrothermal solutions from the southern Juan de Fuca Ridge, J. Geophys. Res. 92 (1987) 11334–11346.

[2] K.L. Von Damm, A.M. Bray, L.G. Buttermore, S.E. Oosting, The geochemical controls on vent fluids from the Lucky Strike vent field, Mid-Atlantic Ridge, Earth Planet. Sci. Lett. 160 (1998) 521–536.

[3] J. Cowan, J. Cann, Supercritical two-phase separation of hydrothermal fluids in the Troodos ophiolite, Nature 333 (1988) 259–261.

[4] K.L. Von Damm, L.G. Buttermore, S.E. Oosting, A.M. Bray, D.J. Fornari, M.D. Lilley, W.C. Shanks III, Direct observation of the evolution of a seafloor 'black smoker' from vapor to brine, Earth Planet. Sci. Lett. 149 (1997) 101–111.

[5] K.L. Von Damm, Chemistry of hydrothermal vent fluids from 9°–11°N. East Pacific Rise: 'Time zero', the immediate posteruptive period, J. Geophys. Res. 105 (2000) 11203–11222.

[6] G.J. Massoth, D.A. Butterfield, J.E. Lupton, R.E. McDuff, M.D. Lilley, I.R. Jonasson, Submarine venting of phase-separated hydrothermal fluids at Axial Volcano Juan de Fuca Ridge, Nature 340 (1989) 702–705.

[7] J.L. Charlou, Y. Fouquet, J.P. Donval, J.M. Auzende, Mineral and gas chemistry of hydrothermal fluids on an ultrafast spreading ridge: East Pacific Rise 17° to 19°S (Naudur cruise, 1993) phase separation processes controlled by volcanic and tectonic activity, J. Geophys. Res. 101 (1996) 15899–15919.

[8] D.A. Butterfield, G.J. Massoth, Geochemistry of North Cleft segment vent fluids: Temporal changes in chlorinity and their possible relation to recent volcanism, J. Geophys. Res. 99 (1994) 4951–4968.

[9] M.E. Berndt, W.E. Seyfried Jr., Boron, bromine and other trace elements as clues to the fate of chlorine in mid-ocean ridge vent fluids, Geochim. Cosmochim. Acta 54 (1990) 2235–2245.

[10] D.A. Butterfield, G.J. Massoth, R.E. McDuff, J.E. Lupton, M.D. Lilley, Geochemistry of hydrothermal fluids from axial seamount hydrothermal emissions study vent field Juan de Fuca Ridge: Subseafloor boiling and subsequent fluid-rock interaction, J. Geophys. Res. 95 (1990) 12895–12921.

[11] Y. Fouquet, J.-L. Charlou, I. Costa, J.-P. Donval, J. Radford-Knoery, H. Pellé, H. Ondréas, N. Lourenço, M. Ségonzac, M.K. Tivey, A detailed study of the Lucky Strike hydrothermal site and discovery of a new hydrothermal site Menez Gwen; Preliminary results of the DIVA1 cruise, InterRidge News 3 (1994) 14–17.

[12] J. Radford-Knoery, J.-L. Charlou, J.-P. Donval, M. Aballéa, Y. Fouquet, H. Ondréas, Distribution of dissolved sulfide, methane and manganese near the seafloor at the Lucky Srike (37°17′N) and Menez Gwen (37°50′N) hydrothermal vent site on the mid-Atlantic Ridge, Deep-Sea Res. I 45 (1998) 367–386.

[13] R. Botz, G. Winckler, R. Bayer, M. Schmitt, M. Schmidt, D. Garbe-Schönberg, P. Stoffers, J.K. Kristjansson, Origin of trace gases in submarine hydrothermal vents of the Kolbeinsey Ridge, north Iceland, Earth Planet. Sci. Lett. 171 (1999) 83–93.

[14] C.S. Chin, G.P. Klinkhammer, C. Wilson, L.A. Lawver, J.E. Lupton, Hydrothermal activity in a Nascent Backarc Basin: The Bransfield Strait, Antarctica, EOS Trans. Am. Geophys. Union 77 (1996) F413.

[15] G.P. Klinkhammer, C.S. Chin, C. Wilson, M.D. Rudnicki, R.A. Keller, M.R. Fisk, L.A. Lawver, Results of a search for hydrothermal activity in the Bransfield Strait Antarctica, EOS Trans. Am. Geophys. Union 78 (1995) F710.

[16] G. Bohrmann, C. Chin, S. Petersen, H. Sahling, U. Schwarz-Schampera, J. Greinert, S. Lammers, G. Rehder, A. Dählmann, K. Wallmann, S. Dijkstra, H.-W. Schenke, Hydrothermal activity at Hook Ridge in the Central Bransfield Basin, Antarctica, Geo-Mar. Lett. 18 (1999) 277–284.

[17] D.H.N. Barker, J.A. Austin Jr., Crustal diapirism in Bransfield Strait, West Antarctica: Evidence for distributed extension in marginal-basin formation, Geology 22 (1994) 657–660.

[18] R. Livermoore, J.C. Balayá, A. Maldonado, J.M. Martínez, C.S. De Galdeano, J.G. Zaldívar, A. Jabaloy, A. Barnolas, L. Somoza, J. Hernández-Molina, E. Sriñach, C. Viseras, Autopsy on a dead spreading center The Phoenix Ridge, Drake Passage, Antarctica, Geology 28 (2000) 607–610.

[19] R.A. Keller, M.R. Fisk, Quarternary marginal basin volcanism in the Bransfield Strait as a modern analogue of the southern Chilean ophiolites, in: L.M. Parson, B.J. Murton, P. Browning (Eds.), Ophiolites and their Modern Oceanic Analogues, Geological Society Special Publication 60, The Geological Society, London, 1992, pp. 155–169.

[20] L.A. Lawver, R.A. Keller, M.R. Fisk, J.A. Strelin, Bransfield Strait Antarctic Peninsula – Active Extension behind a Dead Arc, in: B. Taylor (Ed.), Backarc Basins: Tectonics and Magmatism, Plenum Press, New York, 1995, pp. 315–343.

[21] R.A. Keller, M.R. Fisk, W.M. White, K. Birkenmajer, Isotopic and trace element constraints on mixing and melting models of marginal basin volcanism, Bransfield

Strait, Antarctica, Earth Planet. Sci. Lett. 111 (1991) 287–303.
[22] E. Suess, M. Fisk, D. Kadko, Thermal interaction between back-arc volcanism and basin sediments in the Bransfield Strait, Antarctica, Antarct. J. USA 22 (1987) 47–49.
[23] M.J. Whiticar, E. Suess, Hydrothermal hydrocarbon gases in the sediments of the King George Basin, Bransfield Strait, Antarctica, Appl. Geochem. 5 (1990) 135–147.
[24] M.J. Whiticar, E. Suess, H. Wehner, Thermogenic hydrocarbons in surface sediments of the Bransfield Strait, Antarctic Peninsula, Nature 314 (1985) 87–90.
[25] M. Brault, B.R.T. Simoneit, Mild hydrothermal alteration of immature organic matter in sediments from the Bransfield Strait, Antarctica, Appl. Geochem. 5 (1990) 149–158.
[26] P. Schlosser, E. Suess, R. Bayer, M. Rhein, ^{3}He in the Bransfield Strait waters: indication for local injection from back-arc rifting, Deep-Sea Res. I 35 (1988) 1919–1935.
[27] G.P. Klinkhammer, C.S. Chin, R. Keller, A. Dählmann, H. Sahling, G. Sarthou, S. Petersen, F. Smith, C. Wilson, Discovery of hydrothermal vent sites in Bransfield Strait, Antarctica, Earth Planet. Sci. Lett. 193 (2001) 395–407.
[28] A.G. Dickson, pH buffer for sea water media based on the total hydrogen ion concentration scale, Deep-Sea Res. I 40 (1993) 107–118.
[29] K. Grasshoff, M. Ehrhardt, K. Kremling, Methods of Seawater Analysis, VCH, Weinheim, 1983.
[30] M.J. Mottl, H.D. Holland, Chemical exchange during hydrothermal alteration of basalt by seawater – I. Experimental results for major and minor components of seawater, Geochim. Cosmochim. Acta 42 (1978) 1103–1115.
[31] J.M. Gieskes, J.R. Lawrence, Alteration of volcanic matter in deep sea sediments: evidence from the chemical composition of interstitial waters from deep sea drilling corres, Geochim. Cosmochim. Acta 45 (1981) 1687–1703.
[32] K.L. Von Damm, Seafloor hydrothermal activity: black smoker chemistry and chimneys, Annu. Rev. Earth Planet. Sci. 18 (1990) 173–204.
[33] M.T. VonBreymann, R. Collier, E. Suess, Magnesium adsorption and ion exchange in marine sediments: A multi-component model, Geochim. Cosmochim. Acta 54 (1990) 3295–3313.
[34] J.L. Bischoff, R.J. Rosenbauer, Phase separation in seafloor geothermal systems: an experimental study of the effects on metal transport, Am. J. Sci. 287 (1987) 953–978.
[35] J.L. Bischoff, R.J. Rosenbauer, Liquid-vapour relations in the critical region of the system NaCl-H_2O from 380 to 415°C: A refined determination of the critical point and two-phase boundary of seawater, Geochim. Cosmochim. Acta 52 (1988) 2121–2126.
[36] W.E. Seyfried Jr., M.E. Berndt, D.R. Janecky, Chloride depletions and enrichments in seafloor hydrothermal fluids: Constraints from experimental basalt alteration studies, Geochim. Cosmochim. Acta 50 (1986) 469–475.
[37] W.F. Giggenbach, Isotopic shifts in waters from geothermal and volcanic systems along convergent plate boundaries and their origin, Earth Planet. Sci. Lett. 113 (1992) 495–510.
[38] W.C. Shanks, III, J.K. Böhlke, R.R. Seal, Stable isotopes in mid-ocean ridge hydrothermal systems: interactions between fluids, minerals and organisms, in: S.E. Humphris, R.A. Zierenberg, L.S. Mullineaux, R.E. Thomson (Eds.), Seafloor Hydrothermal Systems, Geophysical Monograph 91, American Geophysical Union, Washington, DC, 1995, pp. 194–221.
[39] J. Alt, Subseafloor processes in mid-ocean ridge hydrothermal systems, in: S. Humphris, R. Zierenberg, L. Mullineaux, R. Thomson (Eds.), Seafloor Hydrothermal Systems, Geophysical Monographs 91, American Geophysical Union, Washington, DC, 1995, pp. 85–114.
[40] A.C. Campbell, J.M. Edmond, Halide systematics of submarine hydrothermal vents, Nature 342 (1989) 168–170.
[41] S.E. Oosting, K.L. Von Damm, Bromide/chloride fractionation in seafloor hydrothermal fluids from 9–10°N East Pacific Rise, Earth Planet. Sci. Lett. 144 (1996) 133–145.
[42] M.E. Berndt, W.E. Seyfried Jr., Calibration of Br/Cl fractionation during subcritical phase separation of seawater: Possible halite at 9 to 10°N East Pacific Rise, Geochim. Cosmochim. Acta 61 (1997) 2849–2854.
[43] K. Von Damm, Controls on the chemistry and temporal variability of seafloor hydrothermal fluids, in: S.E. Humphris, R.A. Zierenberg, L.S. Mullineaux, R.E. Thomson (Eds.), Seafloor Hydrothermal Systems, Geophysical Monograph 91, American Geophysical Union, Washington, DC, 1995, pp. 222–247.
[44] D.A. Butterfield, I.R. Jonasson, G.J. Massoth, R.A. Feely, K.K. Roe, R.E. Embley, J.F. Holden, R.E. McDuff, M.D. Lilley, J.R. Delaney, Seafloor eruptions and evolution of hydrothermal fluid chemistry, Phil. Trans. R. Soc. London A 355 (1997) 369–386.
[45] J.L. Bischoff, R.J. Rosenbauer, Salinity variations in submarine hydrothermal systems by layered double-diffusive convection, J. Geol. 97 (1989) 613–623.
[46] J.L. Bischoff, Densities of liquid and vapors in boiling NaCl-H_2O solutions: A pVTx summary from 300°C to 500°C, Am. J. Sci. 291 (1991) 309–338.
[47] R.M. Haymon, D.J. Fornari, K.L. VonDamm, M.D. Lilley, M.R. Perfit, J.M. Edmond, W.C. Shanks III, R.A. Lutz, J.M. Grebmeier, S. Carbotte, D. Wright, E. McLaughlin, M. Smith, N. Beedle, E. Olson, Volcanic eruption of the mid-ocean ridge along the East Pacific Rise crest 9°45–52′N: Direct submersible observations of seafloor phenomena associated with an eruption event in April, 1991, Earth Planet. Sci. Lett. 119 (1993) 85–101.
[48] P. Van Cappellen, L. Qiu, Biogenic silica dissolution in sediments of the Southern Ocean. I. Solubility, Deep-Sea Res. II 44 (1997) 1109–1128.
[49] Y. Fouquet, R.A. Zierenberg, D.J. Miller et al. (Eds.), Proc. ODP, Init. Reports 169 (Ocean Drilling Program), College Station, TX, 1998.
[50] K.L. Von Damm, J.M. Edmond, C.I. Measures, B. Grant, Chemistry of submarine hydrothermal solutions

at Guaymas Basin, Gulf of California, Geochim. Cosmochim. Acta 49 (1985) 2221–2237.
[51] J.L. Morton, R.A. Zierenberg, C.A. Reiss (Eds.), Geologic, Hydrothermal and Biologic Studies at Escanaba Trough, Gorda Ridge, Offshore Northern California, U.S. Geological Survey, Denver, CO, 1994.
[52] C.-F. You, D.A. Butterfield, A.J. Spivack, J.M. Gieskes, T. Gamo, A.J. Campbell, Boron and halide systematics in submarine hydrothermal systems: Effects of phase separation and sedimentary contributions, Earth Planet. Sci. Lett. 123 (1994) 227–238.